TU Delft

Delft University of Technology

Effect of metakaolin on the autogenous shrinkage of alkali-activated slag-fly ash paste

Li, Zhenming; Liang, Xuhui; Chen, Yun; Ye, Guang

DOI
10.1016/j.conbuildmat.2021.122397

Publication date
2021

Document Version
Final published version

Published in
Construction and Building Materials

Citation (APA)
Li, Z., Liang, X., Chen, Y., & Ye, G. (2021). Effect of metakaolin on the autogenous shrinkage of alkali-activated slag-fly ash paste. *Construction and Building Materials*, *278*, Article 122397. https://doi.org/10.1016/j.conbuildmat.2021.122397

Important note
To cite this publication, please use the final published version (if applicable).
Please check the document version above.

Copyright
Other than for strictly personal use, it is not permitted to download, forward or distribute the text or part of it, without the consent of the author(s) and/or copyright holder(s), unless the work is under an open content license such as Creative Commons.

Takedown policy
Please contact us and provide details if you believe this document breaches copyrights.
We will remove access to the work immediately and investigate your claim.

This work is downloaded from Delft University of Technology.
For technical reasons the number of authors shown on this cover page is limited to a maximum of 10.

Construction and Building Materials 278 (2021) 122397

Contents lists available at ScienceDirect

Construction and Building Materials

journal homepage: www.elsevier.com/locate/conbuildmat

Effect of metakaolin on the autogenous shrinkage of alkali-activated slag-fly ash paste

Zhenming Li [a,*,1], Xuhui Liang [a,1], Yun Chen [a,b], Guang Ye [a,c]

[a] Department of Materials, Mechanics, Management & Design, Faculty of Civil Engineering and Geoscience, Delft University of Technology, Delft, Netherlands
[b] School of Materials Science and Engineering, South China University of Technology, Guangzhou, Guangdong 510640, China
[c] Magnel Laboratory for Concrete Research, Department of Structural Engineering, Ghent University, Ghent, Belgium

HIGHLIGHTS

- Metakaolin is applied to mitigate the autogenous shrinkage of alkali-activated slag and fly ash.
- The reaction products and microstructures are characterized investigated.
- Mechanical properties of the paste are studied.
- Metakaolin has a promising potential to be used as an additive in alkali-activated slag and fly systems.

ARTICLE INFO

Article history:
Received 11 August 2020
Received in revised form 8 January 2021
Accepted 12 January 2021

Keywords:
Alkali-activated materials
Slag
Fly ash
Shrinkage
Metakaolin

ABSTRACT

The high autogenous shrinkage of alkali-activated materials made from slag and fly ash is recognised as a major drawback with regard to the use as construction materials. In this study, metakaolin was introduced into the alkali-activated slag-fly ash (AASF) paste to mitigate the autogenous shrinkage. The shrinkage mitigation mechanism of metakaolin was explained by studying the influences of metakaolin on the microstructure, shrinkage related properties, and mechanical properties of AASF paste. It was found that adding metakaolin could significantly reduce the chemical and autogenous shrinkage of AASF paste. This shrinkage mitigation is accompanied by a decrease in the alkalinity of AASF paste pore solution, a reduced drop in internal relative humidity, and an increase in porosity of AASF paste. Moreover, the incorporation of metakaolin does not change the type of the reaction products, but greatly delays the formation of the reaction products of AASF paste. The addition of metakaolin, above 5% of the binder, results in lower 28-day compressive and flexural strength of AASF paste.

© 2021 The Author(s). Published by Elsevier Ltd. This is an open access article under the CC BY license (http://creativecommons.org/licenses/by/4.0/).

1. Introduction

Alkali activated materials (AAMs) are promising as a desirable alternative to ordinary Portland cement (OPC). In addition to the superior strength and durability, one of the most important advantages of AAMs is the lower CO_2 emission and the less energy consumption involved in the production of AAMs in comparison with OPC [1–3].

A wide range of aluminosilicate materials that are reactive in alkaline environments can be used as precursors to synthesise AAMs [4,5], among which, blast furnace slag and coal fly ash are the most widely utilised industrial by-products. Two types of fly ash have been used for AAMs production, namely high-calcium (Class C) fly ash and low-calcium (Class F) fly ash [6]. Compared with Class C fly ash, Class F fly ash (reactive CaO $\leq$ 10%), due to its wider availability, is more intensively studied in the world and the AAM paste synthesized from Class F fly ash usually exhibits better volume stability [7]. NaOH and/or Na_2SiO_3 are usually used as the activator [8]. Alkali activators with the modulus (SiO_2/Na_2O) in the range of 0.5–1.5 are found to promote the formation of a dense microstructure, resulting in high strength for slag and fly ash-based AAMs [9].

Much research has been conducted to investigate the properties of NaOH and/or Na_2SiO_3 activated slag and fly ash materials, especially their mechanical properties and durability [10,11]. The alkali-activated slag normally shows high strength at ambient temperature [12]. Alkali-activated fly ash systems, by contrast, have very slow strength development at ambient temperature. However, slag-based AAM systems usually set rapidly [13]. It has been reported that the alkali-activated slag and fly ash blended

* Corresponding author.
E-mail address: z.li-2@tudelft.nl (Z. Li).
[1] These authors contributed to this work equally.

https://doi.org/10.1016/j.conbuildmat.2021.122397
0950-0618/© 2021 The Author(s). Published by Elsevier Ltd.
This is an open access article under the CC BY license (http://creativecommons.org/licenses/by/4.0/).

systems show reasonable setting time and good mechanical properties. Therefore, alkali-activated slag and fly ash blends are considered to be more promising for widespread use in engineering, compared with AAMs made from sole slag or fly ash [12,14].

Despite the good durability and mechanical properties of alkali-activated slag-fly ash (AASF), this material usually shows large autogenous shrinkage [15,16]. Autogenous shrinkage is a serious issue for construction materials since it can induce internal tensile stress and consequently micro- or macro- cracking of the concrete. To widen the application of this eco-friendly binder material, the issue of high autogenous shrinkage has to be addressed.

It has been reported that the shrinkage reducing agent (SRA), expansive additive, and nano-additive that are widely used in OPC are not functional or even can cause side effects (e.g. strength loss) when used in AAMs [17–21]. According to Li et al. and Tu et al. [22,23], internal curing with superabsorbent polymers (SAPs) is effective in mitigating the self-desiccation-induced autogenous shrinkage. However, self-desiccation might not be the sole mechanism of the autogenous shrinkage of AAMs [24,25]. It was found that AASF paste can show a considerable amount of shrinkage even under a humidity of 100%, especially at the very early age [24]. That part of shrinkage was related to the fast reaction in the acceleration period and the densification of the pore structure [24]. Metakaolin (MK) as an aluminosilicate material is very reactive upon alkali activation. It has been found that MK can alter the reaction kinetics and microstructure of AAMs made from slag and fly ash [26,27]. Therefore, the addition of MK into AASF systems may mitigate the autogenous shrinkage induced by self-desiccation and other mechanisms. However, this aspect was not considered in previous studies [27–31].

To comprehensively investigate the mitigation effects of MK, the autogenous shrinkage of AASF was considered as two parts, the autogenous shrinkage subjected to self-desiccation (ε_{desic}) and the shrinkage induced by other mechanisms. The later one can be measured as the shrinkage under saturated condition (ε_{satur}). To explain the underlying mechanism, the reaction kinetics, reaction products, pore solution, and pore structures of AASF paste with different amounts of MK were firstly characterised. The influence of MK on the chemical shrinkage and the internal relative humidity (RH), which reflects the extent of self-desiccation, were then studied [32]. The elastic modulus of the paste was measured to reflect the resistance to shrinkage [33,34]. Finally, the mechanical strength of the pastes was measured. The outline of this study is shown in Fig. 1.

2. Materials and methods

2.1. Raw materials and mixture design

The raw materials used in this paper were granulated blast-furnace slag, Class F fly ash and MK. The chemical compositions of the raw materials are shown in Table 1. The mean particle size, d_{50}, of slag, fly ash and MK, was 18.3 μm, 48.1 μm, and 69.4 μm, respectively. Slag, fly ash and MK had a density of 2.9 g/cm^3, 2.4 g/cm^3 and 2.7 g/cm^3, respectively.

The alkaline activator was prepared by mixing anhydrous pellets of sodium hydroxide with deionised water and commercial sodium silicate solution (27.5 wt% SiO_2 and 8.25 wt% Na_2O). The paste mixtures are shown in Table 2. In AASF pastes, slag was replaced by MK at 10 wt% and 20 wt%. This is because introducing more than 20 wt% of MK in AASF system could lead to considerable strength loss according to [27]. The fly ash content was kept at 50 wt% of the binder.

The paste was mixed in a 5 L epicyclical Hobart mixer. The raw materials were premixed for 1 min before the activator was added. The paste was mixed at low speed for 1 min during the addition of activator. Afterwards, the material on the side of the spot was scraped down and the paste was mixed at high speed for another 2 min. The paste for microstructure characterisation was cast into small plastic bottles (diameter of 30 mm and height of 50 mm) and only the core part of the sample was used. The paste for all tests was subject to 2 times of vibration for 30 s each during casting to remove the air bubbles. The curing temperature of the samples was 20° C. All the samples in this paper were sealed during curing.

2.2. Experimental methods

2.2.1. Microstructure characterisation

The pastes were ground into powders and the reaction was stopped by solvent exchange method at 1 day and 7 days [35]. X-ray diffraction (XRD) was performed to detect the possible crystals formed in the paste. A Philips PW 1830 powder X-ray diffractometer, with Cu Kα (1.5406 Å) radiation, tube setting of 40 kV and 40 mA, a step size of 0.030° and a 2θ range of 5–70°, was used to perform the test. The chemical bonds formed within the reaction products were determined by Fourier transform infrared spectroscopy (FTIR) using a Spectrum TM 100 Optical ATR-FTIR spectrometer over the wavelength range of 600 cm^{-1} to 4000 cm^{-1}. The resolution of the measurement was 4 cm^{-1}.

The reaction heat flow of the pastes was measured by isothermal calorimetry using a TAM Air conduction calorimeter. The temperature during the experiment was controlled to be 20 ± 0.02 °C. The detailed procedure can be found in [22]. Both the heat flow and cumulative heat were normalised by the mass of the binder.

Nitrogen absorption is able to detect small pores (from 0.2 to 200 nm) in the paste. The pastes cured for 1 day, 7 days and 28 days were crushed into small pieces (2–4 mm) and the reaction was stopped by solvent exchange method [35]. The relative pressure ranged from 0.05 to 0.99. The isotherms was obtained based on Barrett-Joyner-Halenda models (BJH) [36].

The pore solution of hardened pastes cured for 1 day and 7 days was extracted using the steel-die method. The obtained pore solution was then diluted using nitric acid (0.2 vol%). The diluted solutions were analysed through a PerkinElmer Optima 5300DV ICP-OES spectrometer, by which the elemental concentrations of Na, Ca, Si and Al were determined. The concentration of OH^- in the pore solution was measured by titration against hydrochloride acid (0.1 M). Phenolphthalein was used as the indicator. The average results of three replicates for each sample are presented.

2.2.2. Chemical shrinkage and autogenous shrinkage measurements

Gravimetry was used to measure the chemical shrinkage of the pastes as suggested by [37]. Three replicates were tested for each mixture.

The autogenous shrinkage of the paste was measured by the corrugated tube method according to ASTM C1968 [38]. The shrinkage under saturated condition (ε_{satur}) was measured by a modified corrugated tube method [39,40]. The detailed procedures of the measurements can be found in [24].

2.2.3. Internal RH measurement

Measurements of internal RH in AASF paste were performed by Rotronic hygroscopic DT stations [41]. The dimension of the sample container was 30 mm. The paste was crushed into small pieces around 0.5 cm^3 and the pieces were immediately inserted into the hermetic measuring chambers. For the measurement of the RH of the pore solution, the same sensors were used. Two measurements for each sample were conducted simultaneously at two different HC2-AW measuring cells. The nominal accuracy of the sensors was reported to be within ±1% RH [42]. Calibration of the sensors

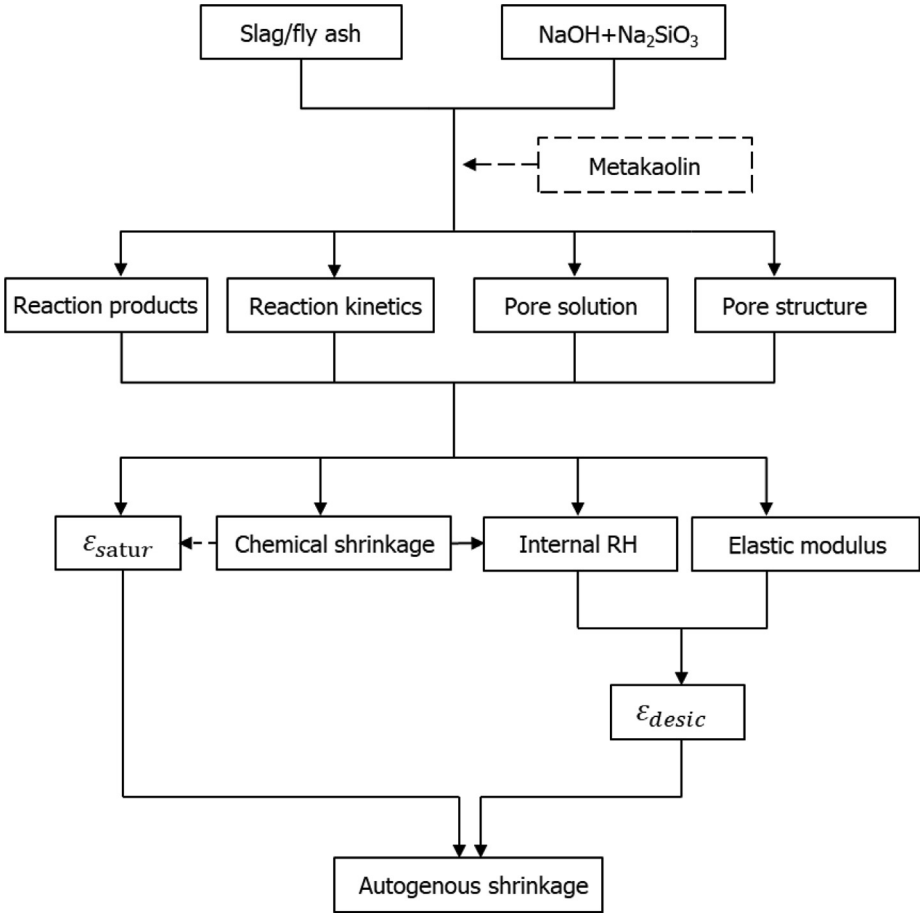

Fig. 1. Outline of this study.

Table 1
Chemical compositions of the raw materials.

Oxide (wt. %)	CaO	Al_2O_3	SiO_2	MgO	Fe_2O_3	SO_3	K_2O	TiO_2	Other	LOI
Slag	40.5	13.3	31.8	9.3	0.5	1.5	0.3	1.0	0.5	1.3
FA	4.8	23.8	56.8	1.5	7.2	0.3	1.6	1.2	1.6	1.2
MK	0.6	38.4	55.1	–	2.6	–	0.2	1.1	0.1	1.9

LOI = Loss on ignition.

Table 2
Mixture design of AASF pastes with different contents of MK.

	Slag (g)	Fly ash (g)	MK (g)	SiO_2 (mol)	Na_2O (mol)	H_2O (g)
S50F50	500	500	–	1.146	1.5	420
S45F50MK5	450	500	50	1.146	1.5	420
S40F50MK10	400	500	100	1.146	1.5	420

was conducted regularly using three standard salt solutions with equilibrium RH at 65%, 80%, and 95%.

2.2.4. Mechanical properties

The elastic modulus of the pastes was tested by a Tonibank Instron. Paste prisms with the size of 40 × 40 × 160 mm^3 were prepared and cured for 1 day and 7 days, before the measurement. Samples were subjected to a load with a constant rate at 0.004 mm/second [43]. The load was controlled and recorded by the Instron, while the displacement was monitored by four transducers (LVDTs) on each side of the prismatic sample. The results were obtained with three replicates for each mixture at each age.

The flexural and compressive strength of the pastes at the age of 1 day, 7 days, and 28 days were measured according to NEN 196-1 [44].

3. Results and discussion

3.1. Microstructure evolution

3.1.1. XRD analysis

Fig. 2 shows the XRD patterns of the precursors and AASF pastes at curing ages of 1 day and 7 days. Slag was mainly amorphous, while fly ash and MK contained a large amount of crystals. The

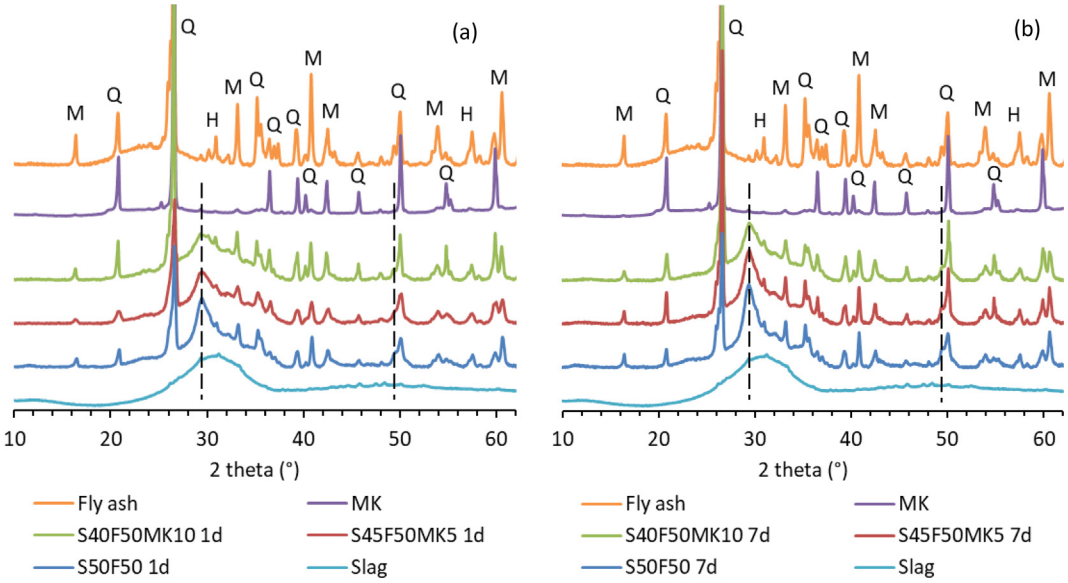

Fig. 2. XRD of AASF pastes cured for (a) 1 day and (b) 7 days, in comparison with the precursors (slag, fly ash and MK). M, Q and H stand for mullite, quartz and hematite, respectively.

crystalline phases in fly ash were mullite ($(Al_2O_3)_{1.136}(SiO_2)_{0.728}$), quartz ($SiO_2$) and hematite ($Fe_2O_3$). MK contained only quartz (SiO_2). The crystalline phases identified in the pastes were from fly ash and MK. Little new crystal was formed within the 7 days of curing. Besides the peaks for crystals, the spectra for the pastes show main bands at 29° (marked by the dashed line), which indicates the formation of C-A-S-H type gel [45]. The intensity of the main band of the paste increases with the curing time, but decreases as the content of MK increases, indicating a lower amount of reaction products due to the incorporation of MK.

3.1.2. FTIR analysis

Fig. 3 shows the FTIR spectra of AASF pastes with different amounts of MK. Several bands can be recognised in the spectra (marked by the dashed lines). The main band at 950 cm^{-1} is attributed to the asymmetrical stretching vibration of Si–O bonds generated in Q^2 units, which is a typical structure of aluminosilicate chains contained in C-A-S-H type gel [46–48]. The band at around 815 cm^{-1} is representative of Si–O symmetric stretching vibrations generated by Q^1 [47]. The bands at around 895 cm^{-1} and 660 cm^{-1} are associated with the deformational vibrations of Si-O-T (T = Si or Al) [46,47].

The same locations of the bands (660, 815, 895, 950, etc. cm^{-1}) detected in different pastes indicate that the same type of reaction product, C-A-S-H gel, was formed in the pastes, irrespective of the presence of MK. The bands at 895 cm^{-1}, 815 cm^{-1}, and 660 cm^{-1} become less intensive with the incorporation of MK, indicating that the amount of reaction products decreased when more MK was present in the paste. This is in line with the XRD results and the results of [27,49].

3.1.3. Heat flow and setting time

The heat flow curves of AASF pastes with different contents of MK are shown in Fig. 4 (a). The initial peak which occurred immediately after the samples were put into the cells corresponded to the initial reactions (mainly dissolution) of the raw materials. After a short dormant period, the main peak appeared, representing the formation of a large amount of reaction products. The main (second) peak corresponded to the acceleration period, the starting time of which is marked by the dashed line in Fig. 4 (a). When slag was replaced by MK, the magnitude of the main peak became lower and the main peak appeared later. For S40F50M10 mixture, the main peak can even hardly be distinguished. The cumulative heat released by the pastes is shown in Fig. 4 (b). AASF pastes released similar heats during the first 5 h. After that, the paste with more MK showed lower heat release. These results indicate the presence of MK can significantly reduce the early-age reaction rate and slightly reduce the total reaction degree of AASF paste. Similar effects of MK were also found for AAS paste [27].

The Vicat setting time results are shown in Table 3. The incorporation of 5% of MK in the binder led to prolonged initial and final setting time, by 15 min and 38 min, respectively. The effect of a higher dosage of MK did not have pronounced further effects on the setting time of the paste.

According to the results of [22,24,50], the shrinkage of AAMs paste in the dormant period is mainly viscous/plastic deformation, which does not generate stress when the material is restrained. The start of the acceleration period of heat flow tested by calorimeter has been suggested more proper as zero time of the autogenous shrinkage of AAMs than the final setting time tested by Vicat. Therefore, the starting times of the acceleration period (4.5 h, 7.5 h and 9.5 h for S50F50, S45F50MK5 and S40F50MK10, respectively, see Fig. 4 (a)) were used as zero times of the autogenous shrinkage in this paper, as will be shown in section 3.2.

3.1.4. Pore solution compositions

Fig. 5 shows the elemental/ions concentrations in the pore solutions of AASF pastes. The concentrations of Na^+ and OH^- in the pore solutions of S45F50MK5 and S40F50MK10 were lower than those in S50F50 at 1 day and 7 days, although the same activator was used for these mixtures. This indicates that the dissolution and the reaction of MK consumed more Na^+ and OH^- than those of slag and fly ash [51]. The concentration of Ca was reduced with the presence of MK, especially at the age of 1 day. The reduction fraction in Ca was around 30% and 55% for 5% and 10% incorporation of MK, respectively. Therefore, the reductions were not simply due to the lower contents of slag. The dissolution of slag was likely hindered due to the presence of MK at the early age. This hypothesise is in line with the calorimetry results (Fig. 4 (a)). Fig. 5 (c) shows that more Si and Al existed in the pore solution of AASF paste with MK, especially at the early age. This was probably contributed by

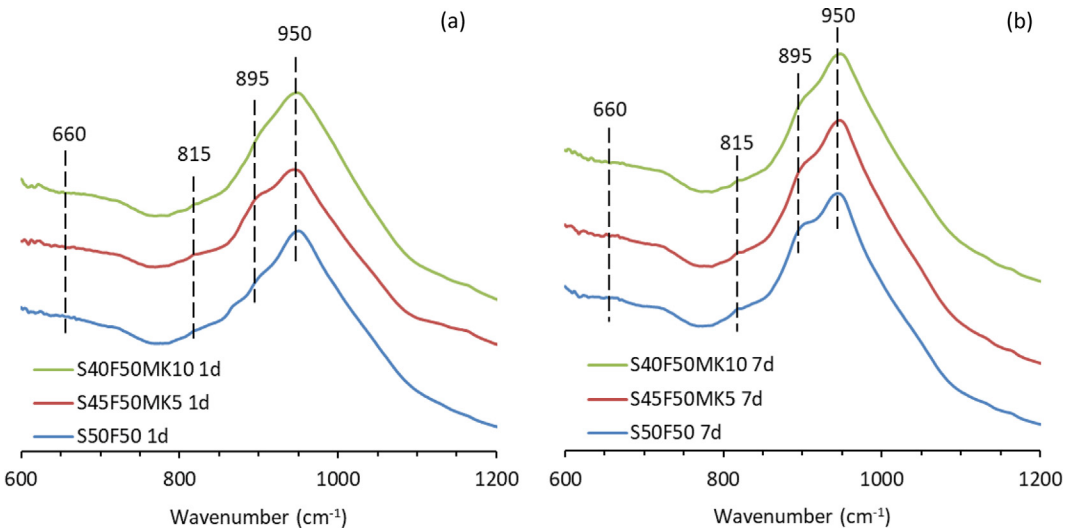

Fig. 3. FTIR spectra of AASF pastes cured for (a) 1 day and (b) 7 days.

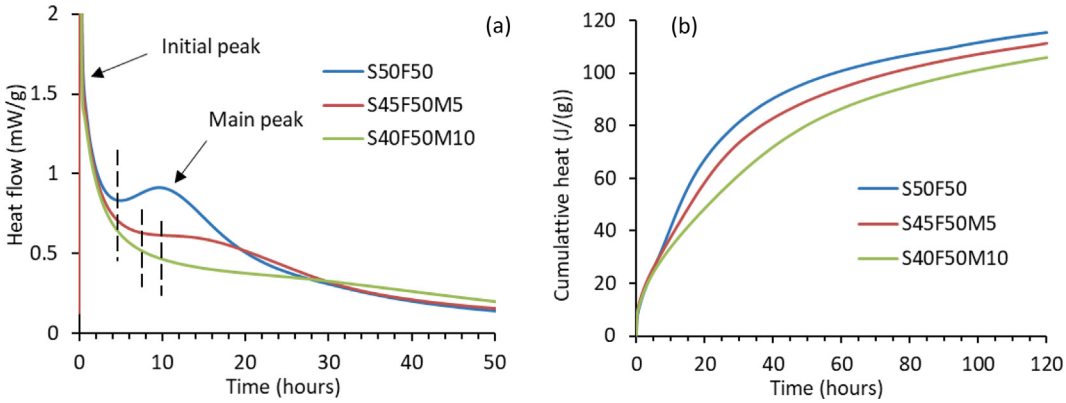

Fig. 4. (a) heat flow and (b) accumulative heat of AASF pastes.

Table 3
Setting times (in min) of AASF pastes.

Mixtures	Initial setting	Final setting
S50F50	117	175
S45F50MK5	132	213
S40F50MK10	133	223

the dissolution of MK whose main chemical compositions were Al_2O_3 and SiO_2 [52].

The differences in the concentrations of ions in different mixture became less evident at 7 days than at 1 day. This is consistent with the FTIR and calorimetry results, which showed that the three AASF systems had similar final reaction products (C-A-S-H gel) and similar overall reaction degrees at the age of 7 days, respectively.

3.1.5. Pore structure

The pore size distribution and differential curves of AASF pastes with different amounts of MK are shown in Fig. 6. The pore sizes detected by N_2 adsorption ranged from 2 nm to around 200 nm. The pores detected at 1 day and 7 days in the paste mainly belonged to capillary pores (>10 nm). The critical pore size was larger than 200 nm, beyond the measuring range of N_2 adsorption. This indicates that a dense pore structure had not formed in AASF paste yet. A larger pore volume of pore size less than 200 nm is observed for the paste with MK especially at the age of 1 day.

At the age of 28 days, the paste with more MK showed a larger pore volume, as illustrated in Fig. 6 (e). Fig. 6 (f) shows that the pastes had similar characteristic pores at around 4 nm, which corresponded to gel pores (2 nm-10 nm [53]). Therefore, it appears that the incorporation of MK resulted in a larger porosity mainly by increasing the number of pores rather than enlarging the critical pore size. Very few capillary pores were detected in the pastes at 28 days, indicating that a dense microstructure had formed in all the paste mixtures.

In general, introducing MK led to a larger porosity in AASF pastes, irrespective of the curing age.

3.1.6. Summary of the impacts of MK on reaction kinetics and microstructure of AASF

Figs. 2 and 3 show that C-A-S-H gel was the main reaction product in blended slag and fly ash system, irrespective of the presence of MK. Little N-A-S-H type gel was found in MK-containing pastes, despite the higher contents of Si and Al. Fig. 4 shows that the reaction rate became lower after adding MK. The dissolution of slag and fly ash and the formation of reaction products were retarded. This is because the dissolution of MK consumes OH^-, which is essential for the dissolution of slag. As a result, the content of Ca^{2+} dissolved from slag decreases (see Fig. 5). Moreover, the dissolution of MK releases

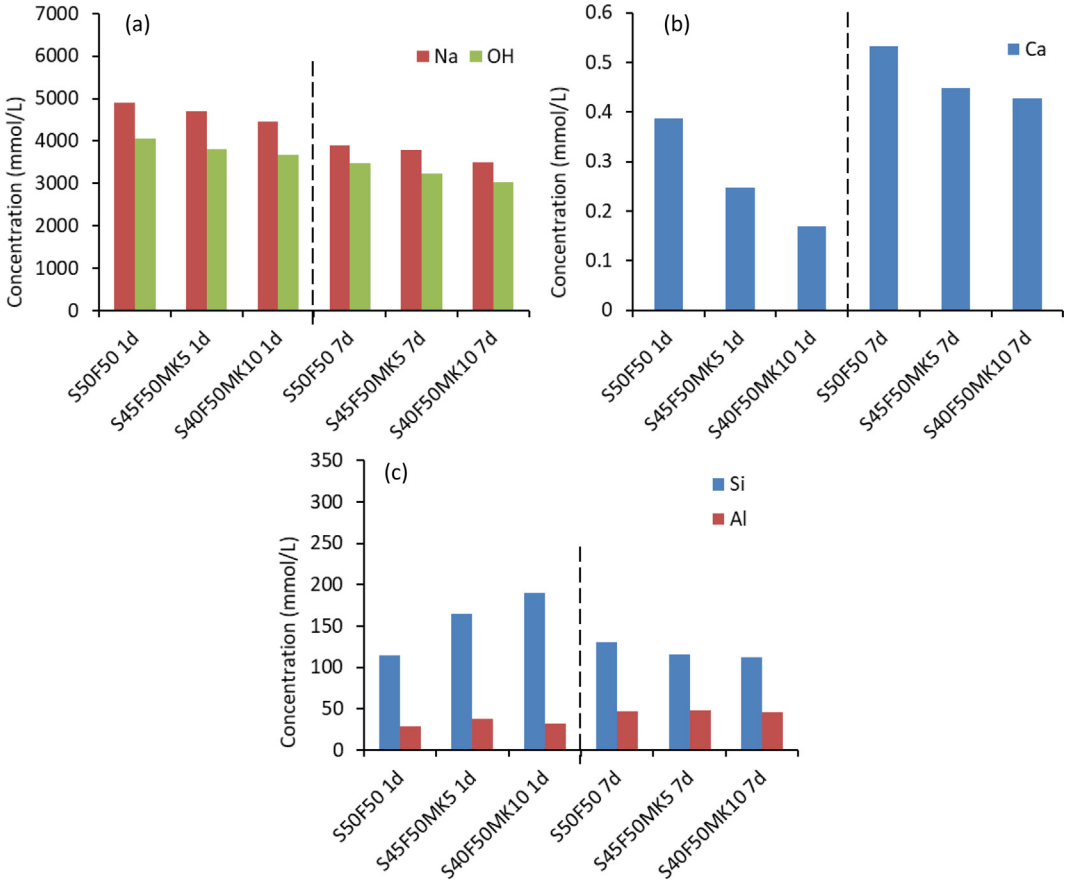

Fig. 5. Concentrations of Na^+ and OH^- (a), Ca (b), Si and Al (c) in the pore solutions of AASF pastes.

extra Si and Al, which reduce the formation rate of CASH gels (Fig. 4) [54–59]. Therefore, the amount of reaction products formed at the early age decreases. The incorporation of MK also prolonged the setting time of AASF paste, as shown in Table 3. Due to the lower reaction rate and the less amount of reaction products formed, a larger porosity was induced for MK-containing pastes, as shown in Fig. 6.

3.2. Autogenous shrinkage

The autogenous shrinkage results are shown in Fig. 7. It can be seen that the plain AASF paste shrank rapidly after the final set. Substituting slag with MK led to a reduction of autogenous shrinkage. If the curves were started at the final setting time, the autogenous shrinkage of S40F50MK10 was 65% and 24% lower than the one of S50F50, at 1 day and 7 days, respectively. Fig. 7 (b) shows the autogenous shrinkage curves, where the starting time of the acceleration period is set as time zero. It can be seen that the shrinkage-mitigating effect of MK was slightly more pronounced than that illustrated in Fig. 7 (a). In the later analysis of this study, only the start of the acceleration period is used as the time-zero of the autogenous shrinkage.

According to [24], the self-desiccation is not the exclusive mechanism of the autogenous shrinkage of AASF. There is a part of the autogenous shrinkage that is irrelevant to the internal RH, especially in the acceleration period [24]. This finding was confirmed by the results reported in [60], which showed a limited mitigating effect of internal curing on the autogenous shrinkage of AASF in the very early age. Hence, it is assumed that the autogenous shrinkage of AASF consists of two parts, as shown in Equation (1).

$$\varepsilon_{as} = \varepsilon_{desic} + \varepsilon_{satur} \quad (1)$$

where ε_{as} is the autogenous shrinkage of the paste; ε_{desic} is the part of the autogenous shrinkage that is induced by self-desiccation; ε_{satur} is the part of the autogenous shrinkage that is irrelevant to internal RH and can be measured in saturated condition.To understand the effects of MK on the autogenous shrinkage of AASF, the effects of MK on these two parts of autogenous shrinkage need to be investigated separately, as presented in the following sections.*3.2.1. Shrinkage under saturated condition*

The shrinkage of AASF pastes under saturated condition is shown in Fig. 8, in comparison with the total autogenous shrinkage as shown in Fig. 7 (b). It can be seen that all pastes showed a certain amount of shrinkage in the saturated condition, especially at the very early age. This phenomenon was not observed in OPC based systems, which would show expansion under saturated conditions due to the formation of expansive crystalline phases [61,62]. After the acceleration period, the development of ε_{satur} became stable probably due to the lowered reaction rate (see Fig. 4). At the age of 1 day, the incorporation of 5% and 10% MK resulted in lower ε_{satur} by 24% and 60%, respectively. The significant reductions on the ε_{satur} by MK contributed to the overall mitigation of the autogenous shrinkage at the early age.

3.2.2. Shrinkage induced by self-desiccation

The shrinkage induced by self-desiccation (ε_{desic}) was calculated using total autogenous shrinkage ε_{as} minus ε_{satur}, as shown in Equation 1. It can be seen from Fig. 9 that ε_{desic} was a big part of the total autogenous shrinkage for all mixtures, especially after the acceleration period. With the incorporation of MK, the self-desiccation-induced autogenous shrinkage was greatly mitigated. For example, at 1 day, the reductions were 60% and 90% for 5% and 10% incorpo-

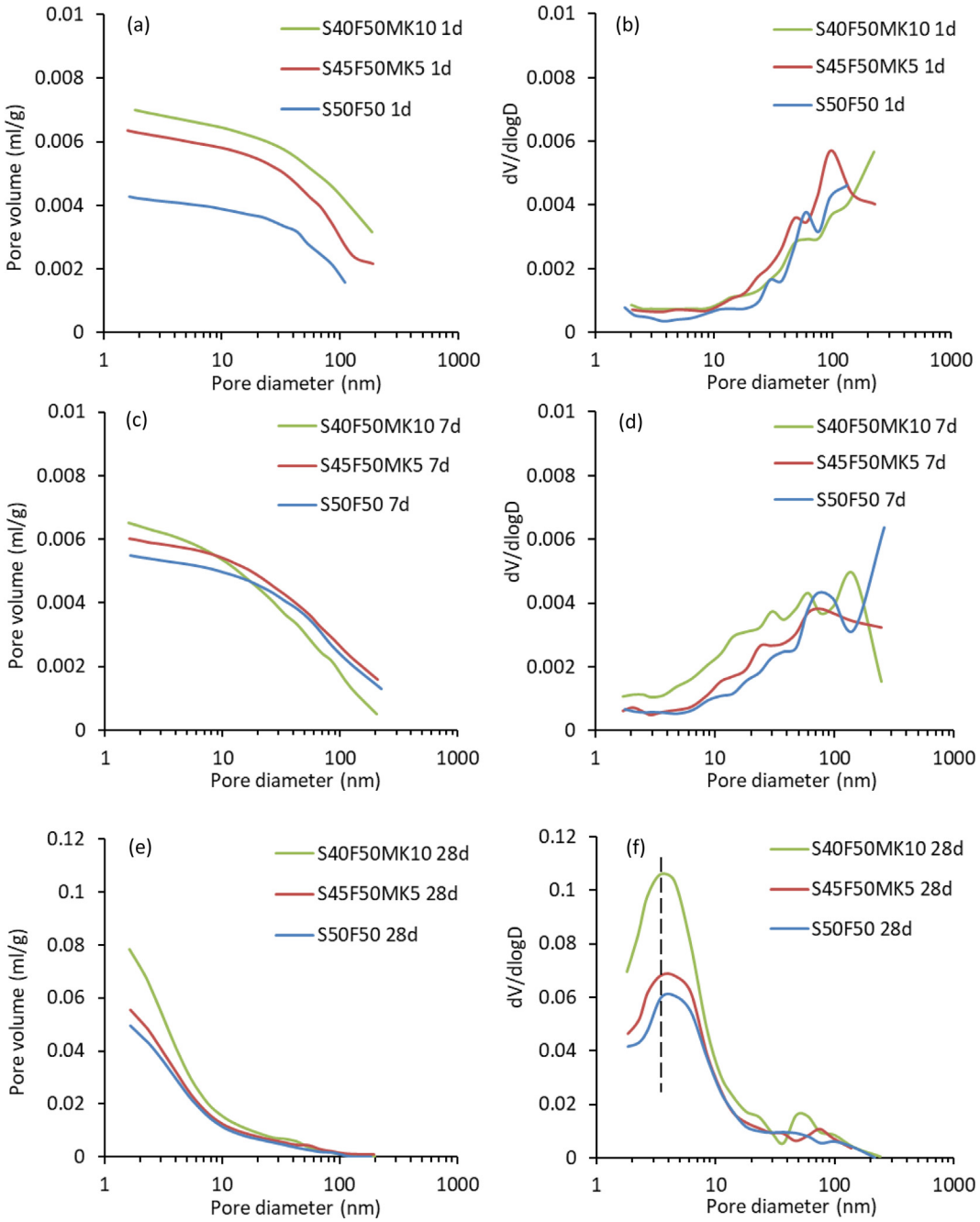

Fig. 6. Pore size distribution and differential curves of AASF pastes cured for 1 day (a,b), 7 days (c,d) and 28 days (e,f).

ration of MK, respectively. At 7 days, the mitigating effect was not as pronounced as in 1 day. This is because the incorporation of MK takes more effects on the reaction kinetics and microstructure of AASF paste at very early age than at late age, as shown in section 3.1. The detailed reason for the mitigating effect of MK on ε_{desic} will be explained based on the results of chemical shrinkage, RH and elastic modulus.

3.2.2.1. Chemical shrinkage. The self-desiccation and the building of liquid–gas menisci in binder materials originate from chemical shrinkage [32,63]. The chemical shrinkage of AASF pastes with different contents of MK is shown in Fig. 10. The record of chemical shrinkage starts from the acceleration period. It can be seen that the chemical shrinkage decreased with the increase in MK content. This was consistent with the reduced reaction rate and the lower amount of reaction products with MK as shown in section 3. Due to chemical shrinkage, internal voids were formed and the pore solution dried gradually from larger pores to smaller pores [32,64]. At the interface between the gas and the liquid, meniscus would form which can generate capillary tension to the pore walls. Given lower chemical shrinkage and higher porosity (Fig. 6) of the paste with MK, the meniscus with a larger diameter would be generated, which meant a higher RH and a smaller force. These points are verified in the next section.

3.2.2.2. Internal RH and pore pressure. The internal RH due to the curvature effect of the meniscus can be calculated according to Equation (2) [63].

$$RH = RH_S \cdot RH_K \quad (2)$$

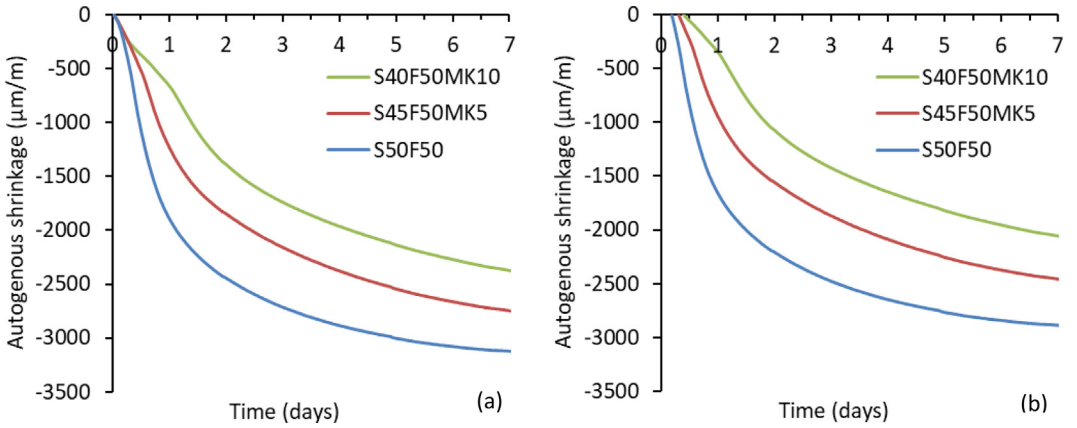

Fig. 7. Autogenous shrinkage of AASF pastes, starting at final setting time tested by Vicat (a) or the start of the acceleration period (b). Detailed results on setting time and heat flow tested by calorimeter are shown in section 3.1.3.

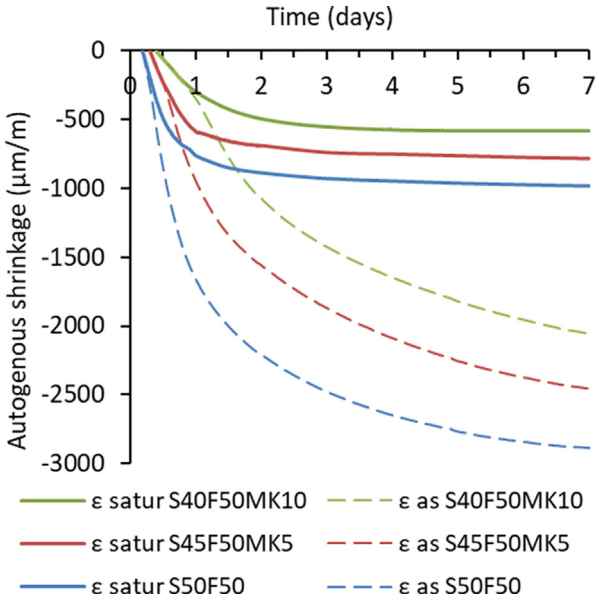

Fig. 8. Shrinkage of AASF pastes under saturated condition (solid lines), with reference to the total autogenous shrinkage (dashed lines).

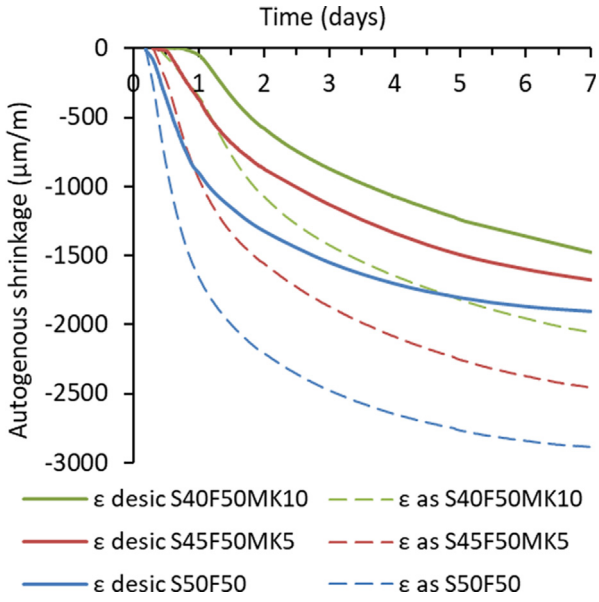

Fig. 9. Shrinkage of AASF pastes induced by self-desiccation (solid lines), with reference to the total autogenous shrinkage (dashed lines).

where RH is the internal RH of the paste, RH_S is the RH caused by the ions in the pore solution and RH_K is the RH caused by the curvature at the gas–liquid interfaces. The measured RH, RH_S and calculated RH_K are shown in Table 4.

With Kelvin equation (Equation (3)) and Laplace equation (Equation (4)), the pore pressure σ (MPa) can be calculated by Equation (5). The calculated pore pressure in AASF paste is also shown in Table 4.

$$\ln(RH_K) = \frac{2\gamma V_w}{rRT} \tag{3}$$

$$\sigma = -\frac{2\gamma}{r} \tag{4}$$

$$\sigma = -\frac{ln(RH_K)RT}{V_w} \tag{5}$$

where γ (N/m) and V_w (m^3/mol) are the surface tension and the molar volume of the pore solution, respectively; r (m) is the radius of the menisci; R (8.314 J/(mol·K)) is the ideal gas constant and T (K) is the absolute temperature, in this paper 293.15 K.

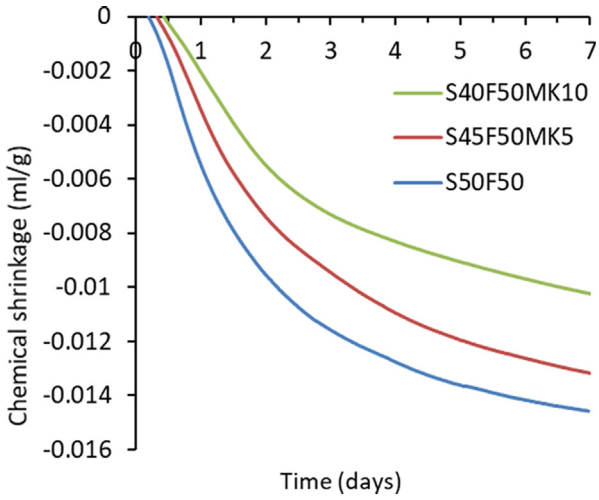

Fig. 10. Chemical shrinkage of AASF pastes, starting at the beginning of the acceleration period.

Table 4
RH and pore pressure in AASF pastes.

Mixture	Specimens cured for 1 day				Specimens cured for 7 days			
	RH(%)	RH_S(%)	RH_K(%)	σ(MPa)	RH(%)	RH_S(%)	RH_K(%)	σ(MPa)
S50F50	81.1	83.2	97.5	3.4	83.6	90.5	92.4	10.7
S45F50MK5	83.4	84.5	98.6	2.0	86.8	91.2	94.5	7.66
S40F50MK10	86.1	87.0	99.0	1.4	91.1	94.8	96.2	5.24

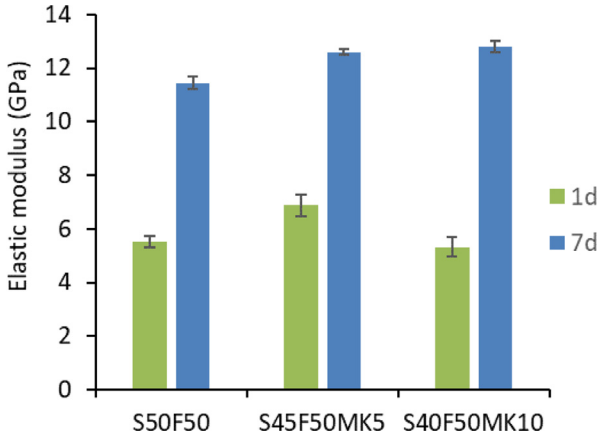

Fig. 11. Elastic modulus of AASF pastes.

The measured RH_S of the pore solutions of AASF pastes were lower than 80% due to the high ion concentrations in the pore solution as shown in Fig. 5 (Raoult's law).

All the three mixtures experienced reductions of RH_K with elapse of time, indicating the occurrence of self-desiccation. The drop in RH_K and the pore pressure was reduced when MK was present. The incorporation of 10% of MK reduced the pore pressure by more than half at 1 day and 7 days.

3.2.2.3. Elastic modulus. The elastic modulus acts as a resistance to the deformation [65]. As shown in Fig. 11, the incorporation of 5% MK into AASF paste resulted in the highest elastic modulus at 1 day. At the age of 7 days, the elastic modulus of all mixtures increased substantially, and S40F50MK10 showed the highest elastic modulus. Nonetheless, the elastic modulus of the three mixtures was not remarkably different.

The similar elastic modulus of the three mixtures indicates that the autogenous shrinkage reduction of AASF paste induced by MK addition can be largely attributed to the reduced driving forces, e.g., pore pressure and steric-hydration force that can develop under saturated condition [24], rather than an increased elastic modulus.

It is worth noticing that the elastic modulus did not decrease with the increase of MK content, although the addition of MK results in a lower amount of reaction products and a larger porosity as shown in section 3.1. This might be due to the mitigating effect of MK on the development of microcracking. According to [66–68], the elastic modulus of AAMs is critically influenced by the development of microcracking. During autogenous shrinkage, the unreacted particles can perform as local restraints which may cause microcracking in the paste [69] and therefore harm the elastic modulus [12,70]. However, the autogenous shrinkage of AASF paste with MK was greatly reduced so that the development of microcracking could be hindered. Thus, the elastic modulus of AASF paste did not decrease with the addition of MK. Indeed, the exposure of the samples to ambient RH (around 50%) during the measurement of the elastic modulus may induce drying shrinkage related microcracking. However, this has not been proved and needs further research.

Since the addition of MK greatly mitigated both ε_{satur} (Fig. 8) and ε_{desic} (Fig. 9) of AASF pastes, the total autogenous shrinkage was reduced as a result. So far the mechanism behind the mitigating effect of MK on the autogenous shrinkage of AASF paste has been clarified.

3.3. Compressive and flexural strength

Besides the autogenous shrinkage, the strength is also an important property for binder materials. As shown in Fig. 12 (a), the incorporation of 5% MK slightly increased the 7-days and 28-days compressive strength of the pastes. However, considering the error range of the experiments, the increase was negligible. When adding 10% of MK, the compressive strength of AASF paste decreased in the whole studied period.

Fig. 12 (b) shows that the 1-day flexural strength of the pastes containing MK was lower than that of the plain AASF paste. However, at the ages of 7 days and 28 days, the flexural strength improved when 5% of MK was added. The incorporation of 10% MK led to higher flexural strength than the plain AASF paste at 7 days but not at 28 days.

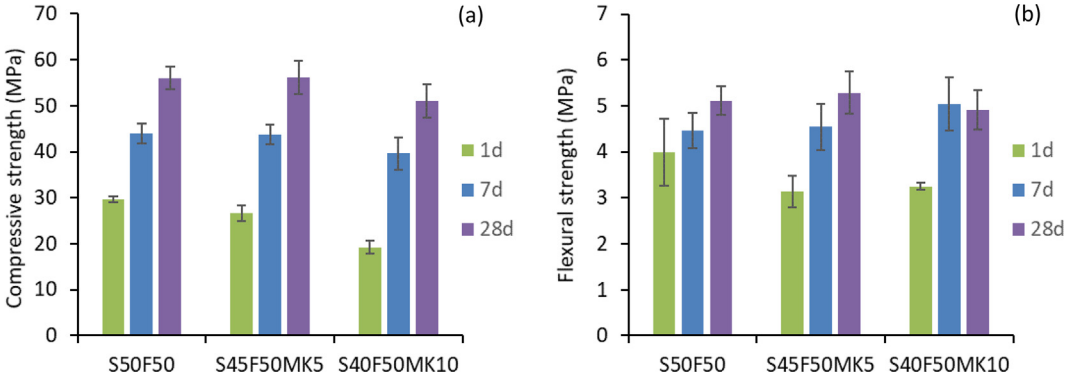

Fig. 12. Compressive strength (a) and flexural strength (b) of AASF pastes.

Based on the results on autogenous shrinkage and mechanical properties of AASF paste with different contents of MK, it seems that the incorporation of MK by 5 wt% of the binder yields the optimal overall performance. A higher amount of MK can induce a decrease in 28-days strength. Nonetheless, the 28-days compressive strength of S40F50MK10, the mixture that shows the lowest strength in this paper, exceeded 50 MPa, which is already adequate for most structural applications [71]. Therefore, a higher amount of MK can be introduced in AASF system for some applications that require enhanced shrinkage-mitigation effects. This study together with previous studies [26,27,72,73] has shown that MK has a promising potential to be utilised in slag and fly ash-based AAMs for performance improvements.

4. Concluding remarks

In this study, the effects of MK incorporation on the microstructure evolution, autogenous shrinkage and mechanical properties of AASF paste were investigated. The mechanism of the shrinkage-reducing effect of MK lies in the modifications of the reaction kinetics and microstructure of AASF pastes. The conclusions are as follows:

1. The incorporation of MK decreased the reaction rate of AASF paste, especially in the acceleration period. As a result, the total amount of reaction products was reduced and the pore refinement was hindered. The setting time of the paste was prolonged when MK was introduced.
2. Due to the reduced chemical shrinkage and the increased porosity, the self-desiccation in AASF paste was mitigated when MK was present. In the meantime, MK did not impact the development of elastic modulus of the paste. As a result, the autogenous shrinkage of AASF induced by self-desiccation was effectively mitigated. The autogenous shrinkage irrelevant to internal RH in AASF was also mitigated by MK.
3. The strength of AASF was barely influenced by the incorporation of 5% of MK in the binder. In contrast, 10% of MK led to a decrease in the 28-days compressive and flexural strength.
4. The mitigated autogenous shrinkage, delayed setting, enhanced elastic modulus and flexure strength indicate that MK has a promising potential to be used in AASF system. However, future research is still needed on the influences of MK on other properties, e.g., the flowability and drying shrinkage of the materials.

CRediT authorship contribution statement

Zhenming Li: Conceptualization, Methodology, Investigation. **Xuhui Liang:** Conceptualization, Methodology, Investigation. **Yun Chen:** Investigation. **Guang Ye:** Project administration.

Declaration of Competing Interest

The authors declare that they have no known competing financial interests or personal relationships that could have appeared to influence the work reported in this paper.

Acknowledgment

The authors would like to acknowledge the funding supported by the China Scholarship Council (CSC) and the grant from the Netherlands Organisation for Scientific Research (NWO). Dr. Hua Dong is acknowledged for the critical reading of the manuscript.

References

[1] R.J. Thomas, H. Ye, A. Radlinska, S. Peethamparan, Alkali-activated slag cement concrete, Concr. Int. 38 (2016) 33–38.
[2] P. Duxson, J.L. Provis, G.C. Lukey, J.S.J. van Deventer, The role of inorganic polymer technology in the development of "green concrete", Cem. Concr. Res. 37 (2007) 1590–1597, https://doi.org/10.1016/j.cemconres.2007.08.018.
[3] G. Habert, C. Ouellet-Plamondon, Recent update on the environmental impact of geopolymers, RILEM Tech. Lett. 1 (2016) 17–23.
[4] S. Songpiriyakij, T. Kubprasit, C. Jaturapitakkul, P. Chindaprasirt, Compressive strength and degree of reaction of biomass- and fly ash-based geopolymer, Constr. Build. Mater. 24 (2010) 236–240, https://doi.org/10.1016/j.conbuildmat.2009.09.002.
[5] S.A. Bernal, E.D. Rodríguez, A.P. Kirchheim, J.L. Provis, Management and valorisation of wastes through use in producing alkali-activated cement materials, J. Chem. Technol. Biotechnol. 91 (2016) 2365–2388.
[6] ASTM C618 - 19, Standard specification for coal fly ash and raw or calcined natural pozzolan for use in concrete, (2008). doi:10.1520/C0618-19.2.
[7] E.I. Diaz, E.N. Allouche, S. Eklund, Factors affecting the suitability of fly ash as source material for geopolymers, Fuel. 89 (2010) 992–996.
[8] J.L. Provis, Activating solution chemistry for geopolymers, in: Geopolymers, Elsevier, 2009, pp. 50–71.
[9] S.-D. Wang, K.L. Scrivener, P.L. Pratt, Factors affecting the strength of alkali-activated slag, Cem. Concr. Res. 24 (1994) 1033–1043.
[10] M.C.G. Juenger, F. Winnefeld, J.L. Provis, J.H. Ideker, Advances in alternative cementitious binders, Cem. Concr. Res. 41 (2011) 1232–1243, https://doi.org/10.1016/j.cemconres.2010.11.012.
[11] K. Arbi, M. Nedeljković, Y. Zuo, G. Ye, A Review on the Durability of Alkali-Activated Fly Ash/Slag Systems: Advances, Issues, and Perspectives, Ind. Eng. Chem. Res. 55 (2016) 5439–5453, https://doi.org/10.1021/acs.iecr.6b00559.
[12] M. Nedeljković, Z. Li, G. Ye, Setting, strength, and autogenous shrinkage of alkali-activated fly ash and slag pastes: effect of slag content, Materials (Basel). 11 (2018) 2121, https://doi.org/10.3390/ma11112121.
[13] S. Wang, X. Pu, K.L. Scrivener, P.L. Pratt, Alkali-activated slag cement and concrete: a review of properties and problems, Adv. Cem. Res. 7 (1995) 93–102, https://doi.org/10.1680/adcr.1995.7.27.93.
[14] J.L. Provis, J.S.J. Van Deventer, Alkali Activ. Mater. (2014), https://doi.org/10.1007/978-94-007-7672-2.
[15] M. Hojati, A. Radlińska, Shrinkage and strength development of alkali-activated fly ash-slag binary cements, Constr. Build. Mater. 150 (2017) 808–816, https://doi.org/10.1016/j.conbuildmat.2017.06.040.
[16] N.K. Lee, J.G. Jang, H.K. Lee, Shrinkage characteristics of alkali-activated fly ash/slag paste and mortar at early ages, Cem. Concr. Compos. 53 (2014) 239–248, https://doi.org/10.1016/j.cemconcomp.2014.07.007.
[17] M. Criado, A. Palomo, A. Fernández-Jiménez, P.F.G. Banfill, Alkali activated fly ash: Effect of admixtures on paste rheology, Rheol. Acta. 48 (2009) 447–455, https://doi.org/10.1007/s00397-008-0345-5.
[18] G. Habert, J.B. D'Espinose De Lacaillerie, N. Roussel, An environmental evaluation of geopolymer based concrete production: Reviewing current research trends, J. Clean. Prod. 19 (2011) 1229–1238, https://doi.org/10.1016/j.jclepro.2011.03.012.
[19] C.A. Rees, J.L. Provis, G.C. Lukey, J.S.J. van Deventer, The mechanism of geopolymer gel formation investigated through seeded nucleation, Colloids Surfaces A Physicochem. Eng. Asp. 318 (2008) 97–105, https://doi.org/10.1016/j.colsurfa.2007.12.019.
[20] F. Collins, J.G. Sanjayan, cracking tendency of alkali-activated slag concrete subjected to restrained shrinkage, Cem. Concr. Res. 30 (2000) 791–798, https://doi.org/10.1016/S0008-8846(00)00243-X.
[21] X. Hu, C. Shi, Z. Zhang, Z. Hu, Autogenous and drying shrinkage of alkali-activated slag mortars, J. Am. Ceram. Soc. (2019) 1–13, https://doi.org/10.1111/jace.16349.
[22] Z. Li, M. Wyrzykowski, H. Dong, J. Granja, M. Azenha, P. Lura, G. Ye, Internal curing by superabsorbent polymers in alkali-activated slag, Cem. Concr. Res. 135 (2020), https://doi.org/10.1016/j.cemconres.2020.106123 106123.
[23] W. Tu, Y. Zhu, G. Fang, X. Wang, M. Zhang, Internal curing of alkali-activated fly ash-slag pastes using superabsorbent polymer, Cem. Concr. Res. 116 (2019) 179–190, https://doi.org/10.1016/j.cemconres.2018.11.018.
[24] Z. Li, T. Lu, X. Liang, H. Dong, J. Granja, M. Azenha, G. Ye, Mechanisms of autogenous shrinkage of alkali-activated slag and fly ash pastes, Cem. Concr. Res. 135 (2020), https://doi.org/10.1016/j.cemconres.2020.106107 106107.
[25] L. Kalina, V. Bílek, E. Bartoníčková, M. Kalina, J. Hajzler, R. Novotný, Doubts over capillary pressure theory in context with drying and autogenous shrinkage of alkali-activated materials, Constr. Build. Mater. 248 (2020), https://doi.org/10.1016/j.conbuildmat.2020.118620.
[26] S.A. Bernal, J.L. Provis, V. Rose, R. Mejía De Gutierrez, Evolution of binder structure in sodium silicate-activated slag-metakaolin blends, Cem. Concr. Compos. 33 (2011) 46–54, https://doi.org/10.1016/j.cemconcomp.2010.09.004.
[27] Z. Li, M. Nedeljković, B. Chen, G. Ye, Mitigating the autogenous shrinkage of alkali-activated slag by metakaolin, Cem. Concr. Res. 122 (2019) 30–41, https://doi.org/10.1016/j.cemconres.2019.04.016.
[28] C.K. Yip, G.C. Lukey, J.S.J. Van Deventer, The coexistence of geopolymeric gel and calcium silicate hydrate at the early stage of alkaline activation, Cem. Concr. Res. 35 (2005) 1688–1697, https://doi.org/10.1016/j.cemconres.2004.10.042.

[29] A. Buchwald, H. Hilbig, C. Kaps, Alkali-activated metakaolin-slag blends - Performance and structure in dependence of their composition, J. Mater. Sci. 42 (2007) 3024–3032, https://doi.org/10.1007/s10853-006-0525-6.
[30] S.A. Bernal, E.D. Rodríguez, R. Mejıa De Gutiérrez, M. Gordillo, J.L. Provis, Mechanical and thermal characterisation of geopolymers based on silicate-activated metakaolin/slag blends, J. Mater. Sci. 46 (2011) 5477–5486. doi:10.1007/s10853-011-5490-z.
[31] A. Buchwald, R. Tatarin, D. Stephan, Reaction progress of alkaline-activated metakaolin-ground granulated blast furnace slag blends, J. Mater. Sci. 44 (2009) 5609–5617, https://doi.org/10.1007/s10853-009-3790-3.
[32] O.M. Jensen, P.F. Hansen, Autogenous deformation and RH-change in perspective, Cem. Concr. Res. 31 (2001) 1859–1865, https://doi.org/10.1016/S0008-8846(01)00501-4.
[33] F. Collins, J. Sanjayan, Effect of pore size distribution on drying shrinking of alkali-activated slag concrete, Cem. Concr. Res. 30 (2000) 1401–1406, https://doi.org/10.1016/S0008-8846(00)00327-6.
[34] B.D. Kumarappa, S. Peethamparan, M. Ngami, Autogenous shrinkage of alkali activated slag mortars: Basic mechanisms and mitigation methods, Cem. Concr. Res. 109 (2018) 1–9, https://doi.org/10.1016/j.cemconres.2018.04.004.
[35] K. Scrivener, R. Snellings, B. Lothenbach, A practical guide to microstructural analysis of cementitious materials, Crc Press, 2016.
[36] E.P. Barrett, L.G. Joyner, P.P. Halenda, The determination of pore volume and area distributions in porous substances. I. Computations from nitrogen isotherms, J. Am. Chem. Soc. 73 (1951) 373–380.
[37] Z. Li, S. Zhang, Y. Zuo, W. Chen, G. Ye, Chemical deformation of metakaolin based geopolymer, Cem. Concr. Res. 120 (2019) 108–118, https://doi.org/10.1016/j.cemconres.2019.03.017.
[38] ASTM C1968, Standard Test Method for Autogenous Strain of Cement Paste and Mortar, (2013) 1–8. doi:10.1520/C1698-09.2.
[39] Q. Tian, O.M. Jensen, Measurement with corrugated tubes of early-age autogenous shrinkage of cement-based materials, J. Chinese Ceram. Soc. 37 (2009) 39–45.
[40] Z. Li, P. Gao, G. Ye, Experimental study on autogenous deformation of metakaolin based geopolymer, in: 2nd Int. RILEM/COST Conf. Early Age Crack. Serv. Cem. Mater. Struct., Brussels, 2017: pp. 209–214.
[41] O.M. Jensen, P.F. Hansen, Autogenous relative humidity change in silica fume-modified cement paste, Adv. Cem. Res. 7 (1995) 33–38.
[42] H. Huang, G. Ye, Examining the "time-zero" of autogenous shrinkage in high/ultra-high performance cement pastes, Cem. Concr. Res. 97 (2015) 107–114, https://doi.org/10.1016/j.cemconres.2017.03.010.
[43] B. Delsaute, C. Boulay, J. Granja, J. Carette, M. Azenha, C. Dumoulin, G. Karaiskos, A. Deraemaeker, S. Staquet, Testing Concrete E-modulus at Very Early Ages Through Several Techniques: An Inter-laboratory Comparison, Strain. (2016) 91–109, https://doi.org/10.1111/str.12172.
[44] NEN-EN 196-1, Methods of Testing Cement–Part 1: Determination of Strength, 2005, Eur. Comm. Stand. (2005).
[45] M. Ben Haha, G. Le Saout, F. Winnefeld, B. Lothenbach, Influence of activator type on hydration kinetics, hydrate assemblage and microstructural development of alkali activated blast-furnace slags, Cem. Concr. Res. 41 (2011) 301–310, https://doi.org/10.1016/j.cemconres.2010.11.016.
[46] I. Garcia-Lodeiro, A. Palomo, A. Fernández-Jiménez, D.E. MacPhee, Compatibility studies between N-A-S-H and C-A-S-H gels. Study in the ternary diagram Na2O-CaO-Al2O3-SiO2-H2O, Cem. Concr. Res. 41 (2011) 923–931, https://doi.org/10.1016/j.cemconres.2011.05.006.
[47] I. García Lodeiro, A. Fernández-Jimenez, A. Palomo, D.E. Macphee, Effect on fresh C-S-H gels of the simultaneous addition of alkali and aluminium, Cem. Concr. Res. 40 (2010) 27–32, https://doi.org/10.1016/j.cemconres.2009.08.004.
[48] I. García-Lodeiro, A. Fernández-Jiménez, M.T. Blanco, A. Palomo, FTIR study of the sol-gel synthesis of cementitious gels: C-S-H and N-A-S-H, J. Sol-Gel Sci. Technol. 45 (2008) 63–72, https://doi.org/10.1007/s10971-007-1643-6.
[49] S.A. Bernal, J.L. Provis, V. Rose, R.M. De Gutiérrez, High-resolution X-ray diffraction and fluorescence microscopy characterization of alkali-activated slag-metakaolin binders, J. Am. Ceram. Soc. 96 (2013) 1951–1957, https://doi.org/10.1111/jace.12247.
[50] Y. Ma, X. Yang, J. Hu, Z. Zhang, H. Wang, Accurate determination of the "time-zero" of autogenous shrinkage in alkali-activated fly ash/slag system, Compos. Part B Eng. (2019) 107367, https://doi.org/10.1016/J.COMPOSITESB.2019.107367.
[51] J. Davidovits, Geopolymer Chemistry & Applications, 4 th, Institut Géopolymère, Saint-Quentin, France, 2015.
[52] Z. Li, G. Ye, Experimental study of the chemical deformation of metakaolin based geopolymer, in: SynerCrete'18 Int. Conf. Interdiscip. Approaches Cem. Mater. Struct. Concr., Funchal, 2018, pp. 443–448.
[53] K. van Breugel, Simulation of hydration and Formation of Structure in Hardening Cement-Based Materials, (1991) 295.
[54] X. Gao, Q.L. Yu, H.J.H. Brouwers, Reaction kinetics, gel character and strength of ambient temperature cured alkali activated slag-fly ash blends, Constr. Build. Mater. 80 (2015) 105–115, https://doi.org/10.1016/j.conbuildmat.2015.01.065.
[55] N.K. Lee, H.K. Lee, Reactivity and reaction products of alkali-activated, fly ash/slag paste, Constr. Build. Mater. 81 (2015) 303–312, https://doi.org/10.1016/j.conbuildmat.2015.02.022.
[56] D. Ravikumar, N. Neithalath, Reaction kinetics in sodium silicate powder and liquid activated slag binders evaluated using isothermal calorimetry, Thermochim. Acta. 546 (2012) 32–43, https://doi.org/10.1016/j.tca.2012.07.010.
[57] D. Krizan, B. Zivanovic, Effects of dosage and modulus of water glass on early hydration of alkali-slag cements, Cem. Concr. Res. 32 (2002) 1181–1188, https://doi.org/10.1016/S0008-8846(01)00717-7.
[58] I. Ismail, S.A. Bernal, J.L. Provis, R. San Nicolas, S. Hamdan, J.S.J. Van Deventer, Modification of phase evolution in alkali-activated blast furnace slag by the incorporation of fly ash, Cem. Concr. Compos. 45 (2014) 125–135. doi:10.1016/j.cemconcomp.2013.09.006.
[59] M. Ben Haha, B. Lothenbach, G. Le Saout, F. Winnefeld, Influence of slag chemistry on the hydration of alkali-activated blast-furnace slag - Part II: Effect of Al2O3, Cem. Concr. Res. 42 (2012) 74–83, https://doi.org/10.1016/j.cemconres.2011.08.005.
[60] Z. Li, S. Zhang, X. Liang, G. Ye, Internal curing of alkali-activated slag-fly ash paste with superabsorbent polymers, Constr. Build. Mater. 263 (2020), https://doi.org/10.1016/j.conbuildmat.2020.120985 120985.
[61] S. Nagataki, H. Gomi, Expansive admixtures (mainly ettringite), Cem. Concr. Compos. 20 (1998) 163–170.
[62] M.D. Cohen, Theories of expansion in sulfoaluminate-type expansive cements: schools of thought, Cem. Concr. Res. 13 (1983) 809–818.
[63] P. Lura, O.M. Jensen, K. Van Breugel, Autogenous shrinkage in high-performance cement paste: An evaluation of basic mechanisms, Cem. Concr. Res. 33 (2003) 223–232, https://doi.org/10.1016/S0008-8846(02)00890-6.
[64] H. Chen, M. Wyrzykowski, K. Scrivener, P. Lura, Prediction of self-desiccation in low water-to-cement ratio pastes based on pore structure evolution, Cem. Concr. Res. 49 (2013) 38–47, https://doi.org/10.1016/j.cemconres.2013.03.013.
[65] P. Lura, Autogenous Deformation and Internal Curing of Concrete, Delft University of Technology, 2003.
[66] S. Prinsse, D.A. Hordijk, G. Ye, P. Lagendijk, M. Luković, Time-dependent material properties and reinforced beams behavior of two alkali-activated types of concrete, Struct. Concr. 21 (2020) 642–658, https://doi.org/10.1002/suco.201900235.
[67] F.C.S. Carvalho, C.-N. Chen, J.F. Labuz, Measurements of effective elastic modulus and microcrack density, Int. J. Rock Mech. Min. Sci. 34 (1997) 43–e1.
[68] Z. Li, S. Zhang, X. Liang, G. Ye, Cracking potential of alkali-activated slag and fly ash concrete subjected to restrained autogenous shrinkage, Cem. Concr. Compos. 114 (2020), https://doi.org/10.1016/j.cemconcomp.2020.103767 103767.
[69] P. Lura, O.M. Jensen, J. Weiss, Cracking in cement paste induced by autogenous shrinkage, Mater. Struct. 42 (2009) 1089–1099, https://doi.org/10.1617/s11527-008-9445-z.
[70] A. Wardhono, C. Gunasekara, D.W. Law, S. Setunge, Comparison of long term performance between alkali activated slag and fly ash geopolymer concretes, Constr. Build. Mater. 143 (2017) 272–279.
[71] British Standards Institution, Eurocode 2: Design of concrete structures: Part 1-1: General rules and rules for buildings, British Standards Institution, 2004.
[72] S.A. Bernal, R. Mejía De Gutiérrez, J.L. Provis, Engineering and durability properties of concretes based on alkali-activated granulated blast furnace slag/metakaolin blends, Constr. Build. Mater. 33 (2012) 99–108, https://doi.org/10.1016/j.conbuildmat.2012.01.017.
[73] Z. Shi, C. Shi, J. Zhang, S. Wan, Z. Zhang, Z. Ou, Alkali-silica reaction in waterglass-activated slag mortars incorporating fly ash and metakaolin, Cem. Concr. Res. 108 (2018) 10–19, https://doi.org/10.1016/j.cemconres.2018.03.002.